J. Fluid Mech. (1998), *vol.* 356, *pp.* 1–24. Printed in the United Kingdom

From quasi-geostrophic to strongly nonlinear monopolar vortices in a paraboloidal shallow-water-layer experiment

By A. STEGNER[1,2] AND V. ZEITLIN[1]

[1] Laboratoire de Météorologie Dynamique, BP 99 Université Paris 6, 4 place Jussieu, 75252 Paris Cedex 5, France

[2] Laboratoire de Physique Statistique, Ecole Normale Supérieure, 24 rue Lhomond, 75005 Paris, France

(Received 6 January 1997 and in revised form 28 July 1997)

We perform a detailed experimental study of large-scale vortices propagating in the rotating shallow-water layer in a paraboloidal vessel. A specific data acquisition technique is used in order to ensure precise measurements of the free-surface elevation. We find two qualitatively different types of vortex behaviour controlled by the relative elevation value. For small elevations we observe a standard quasi-geostrophic pattern with an asymmetric secondary circulation around an initially symmetric vortex which leads to a meridional drift and Rossby wave radiation. This type of behaviour is exhibited by both cyclonic and anticyclonic vortices. For relative elevations larger than 1 (nonlinear regime) the necessarily anticyclonic vortices are drifting strictly zonally maintaining their circular symmetry during the viscous decay. By varying the initial latitude of the vortex we were able to check that in the nonlinear regime the vortex lifetime is not sensitive to the beta-effect, while it is the case in the quasi-geostrophic regime. In the same way we show that the observed difference in cyclone–anticyclone lifetimes is not influenced by the beta-effect.

1. Introduction

Rotating shallow water (RSW) is one of the prototype models in geophysical fluid dynamics (GFD). It contains the most typical atmospheric/oceanic dynamical ingredients such as rapid weakly dispersive gravity waves, strongly dispersive Rossby waves (in the case of non-uniform Coriolis parameter), slow vortex motions, and interactions among them. However, the very richness of this model makes a direct analysis of the basic equations of motion (primitive equations) very difficult by the obvious reason that it is necessary to cope with motions of very different temporal and spatial scales simultaneously. A traditional approach for this kind of problem which is typical, e.g. for observational data assimilation and meteorological forecast, consists in filtering out the fast motions and describing the long-time evolution in terms of the balanced slow motion. A number of the so-called intermediate or balanced models arise in this way in GFD (McWilliams & Gent 1980) and, in particular, in RSW, being normally based on the geostrophic balance (Warn *et al.* 1995 and references therein). In the case of motions with well-defined characteristic scales as, for instance, a single vortex the most direct method to deduce an intermediate model is a straightforward asymptotic expansion in relevant small parameters. An essential advantage of such models is that they provide a closed evolution equation for a single scalar quantity, normally the pressure (i.e. the free surface elevation in the case of RSW). On one hand,

this quantity could be controlled observationally (e.g. by the satellite altimetry in the oceanic context) and, on the other hand, its evolution equation is easier to integrate numerically than the original primitive equations. As to the validity of the intermediate models, the best way to check their predictions would be to confront them with observations and with direct numerical simulations of the primitive equations. As the first are sparse and not always easy to interpret and the second are still not very reliable, especially for long-time calculations, one may also envisage some laboratory tests. Among them, a study of dynamics of the large-scale monopolar vortices is the most simple way to test the intermediate models results. The purpose of the present paper is an experimental investigation of this kind and our main goal is to demonstrate, in the same experiment, a continuous transition between the patterns of dynamical behaviour which can be, respectively, described by two different intermediate models.

As far as the experiment is concerned, two approaches to study the evolution of barotropic monopolar vortices have been known up to now. In the first, a slow rotating tank with a sloping bottom has been used to mimic a non-uniform Coriolis parameter (Firing & Beardsley 1976†; Masuda, Marubayashi & Ishibashi 1990; Carnevale, Kloosterziel & van Heijst 1991). For slow rotation (5 to 20 r.p.m.) the motion of an isolated geostrophically balanced vortex (i.e. that with a small Rossby number) cannot sustain a strong radial pressure gradient because the Coriolis force is weak. Therefore, for such a vortex the free surface deviation from hydrostatic equilibrium is small. In general such experiments are well described by the standard quasi-geostrophic (QG) model resulting in the well-known streamfunction evolution equation (Pedlosky 1987). Much of the numerical (McWilliams & Flierl 1979; Mied & Lindemann 1979; Sutyrin *et al*. 1994) and theoretical (Sutyrin & Flierl 1994; Reznik & Dewar, 1994) effort has been focused on the study of the evolution of an isolated monopolar barotropic QG vortex on the beta-plane. The main result was that such a vortex produces an asymmetric circulation (the so-called beta-gyres) which, in turn, results in a pronounced meridional component of the drift velocity and Rossby wave radiation.

In the second approach, in the pioneering experiments by Nezlin and co-workers (Antipov *et al*. 1982; Nezlin & Snezhkin 1993) a fast rotating (about 70 r.p.m.) parabolic vessel was used in order to get a curved shallow-water layer (to our knowledge, the idea of using a parabolic device was first discussed by Petviashvili 1980). As the free surface of a rotating fluid assumes a parabolic shape, the angular velocity of rotation may be adjusted in order to get an approximately uniform layer. Hence, as the normal component of the angular velocity depends on latitude, one naturally gets a gradient in the Coriolis parameter. In such an experiment a vortical perturbation of the RSW results in strong deviations of the free surface due to the fast rotation if the layer is thin enough. Dynamical properties of those vortices will be then significantly different from those given by the standard QG model and, in fact, long-lived westward drifting isolated vortices manifesting a cyclone–anticyclone asymmetry were observed by the above-mentioned authors.

In Nature, large-scale monopolar vortices maintaining their coherence for very long times are quite frequent (Lai & Richardson 1977; Ebbesmeyer *et al*. 1986; Brundage & Dugan 1986; Smith *et al*. 1979, 1982, 1989; Mac Low & Ingersoll 1986). They are, thus, natural candidates for application of the ideas of balanced motion, although at the present stage one cannot exclude alternative hypotheses of forced-dissipative structures (Read & Hide 1983; Busse 1994) or inertial structures interacting with a background shear (Meyers, Sommeria & Swinney 1989) where Rossby wave emission

† These authors used a rapidly rotating tank with rigid lid and bottom; as there was no free surface the standard QG model with infinite radius of deformation was still valid.

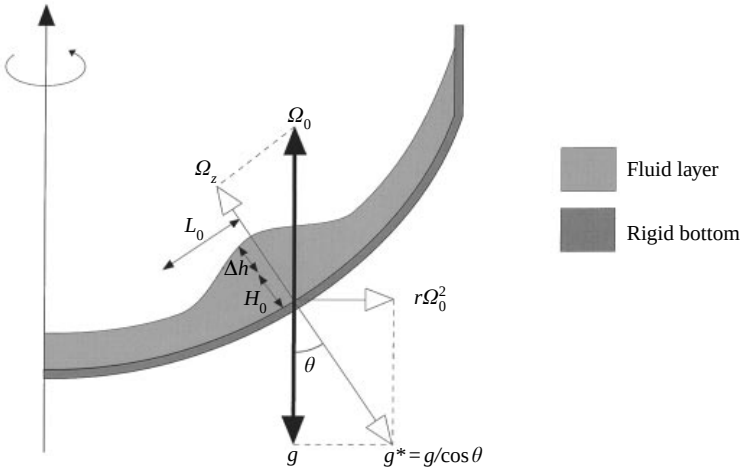

FIGURE 1. Barotropic shallow-water layer in the paraboloidal geometry.

is suppressed by uniformization of the potential vorticity due to the turbulent mixing (Marcus 1990; see Sommeria *et al*. 1991). One may ask, therefore, whether RSW which is representative of the basic dynamical features, could support long-living solitary vortex structures. Owing to the above-mentioned effects of the beta-gyres and Rossby-wave radiation it is impossible to explain the long-time coherence of the monopolar vortices in the framework of the standard QG model. However, as already mentioned, this latter is not the only balanced model consistent with the RSW equation: an entire hierarchy of intermediate models exists (Romanova & Zeitlin 1984; Williams & Yamagata 1984; Williams 1985; Sutyrin 1985; Cushman-Roisin 1986) depending on the characteristic parameters of the vortex. These models are, perhaps, less well known than the standard QG model, but the important fact first noticed by Petviashvili (1980) and Mikhailova & Shapiro (1980) and then studied in detail in Williams & Yamagata (1984), Romanova & Zeitlin (1984, 1985), Sutyrin & Yushina (1988) and Stegner & Zeitlin (1995, 1996) is that a range of parameters exists where a nonlinear anticyclonic vortex of a special form can live for a long time, drifting strictly westward in the planetary geometry. The physical reason for the existence of such a solution, at least in the axisymmetric case, is a mutual compensation of weak nonlinearity (a so-called scalar nonlinearity) and weak dispersion like in the case of the KdV equation (see, however, a recent paper by Kukharkin & Orszag (1996) where the existence of non-symmetric localized vortices in the presence of an unstable shear was established numerically in the same kind of model). That is why it was called a Rossby soliton by some authors, although the collisions among such solitons are not elastic. Up to now, no direct numerical check of this prediction has been made in the framework of the primitive equations. At the same time, as already mentioned, long-lived coherent vortices were observed and identified with Rossby solitons in the fast rotating parabolic vessel experiments (Antipov *et al*. 1981; Nezlin & Snezhkin 1993; Nezlin *et al*. 1996). But, as was first mentioned in Nycander (1993), a fundamental difference exists between the spherical planetary geometry and the experimental paraboloidal geometry. For this latter, the effective gravity g^*, which includes gravitational and centrifugal acceleration, has a latitude dependence, as shown in figure 1. This fact leads to important differences concerning the scalar nonlinearity in the evolution equation in question (Nycander 1993). Without formally proving or disproving the existence of the Rossby solitons on the paraboloid a formula based on centre-of-mass arguments

and relating the drift velocity of such a soliton was given by Nycander (1993). Later, by means of an asymptotic analysis it was shown (Stegner & Zeitlin 1995, 1996) that the changes due to geometry in the evolution equations have a drastic influence on their solutions and the Rossby soliton as defined above does not exist in the intermediate models with paraboloidal geometry. On the contrary, the lifetime of any strongly nonlinear axisymmetric vortex is very long. Such strongly nonlinear regimes correspond to the planetary frontal dynamics regime which was discussed in the atmospheric and oceanic context by Williams & Yamagata (1984) and Cushman-Roisin (1986).

The aim of the present paper is to verify experimentally the predictions of the intermediate models for the behaviour of large-scale slowly evolving (balanced) monopolar vortices in RSW using the same paraboloidal device as in Nezlin & Snezhkin (1993). We pay particular attention to the accurate control of the parameters of the vortices and, in the first place, to the free surface elevation. For this, we have chosen a data acquisition technique, different from Nezlin's experiments, which allows us to directly control and measure the elevation of the free surface (a sort of 'satellite altimetry' has been used). By performing numerous experiments we were able to study vortices for a wide range of parameters in a quantitative way and to establish that two different regimes of vortex behaviour exist. They are controlled by the relative elevation value and are consistent with the intermediate model results

2. Physical parameters in the paraboloidal geometry

In this section, we recall the standard shallow-water beta-plane approximations and the geostrophic balance assumption, from which we extract the physical parameters used in both theoretical and experimental investigations of the paraboloidal shallow-water layer.

The shallow-water approximation is based on the smallness of the thickness parameter $\delta = H_0/L_0 \ll 1$, and the smallness of the vertical velocity $V_z/V_0 = \delta$, where L_0, V_0 and H_0, V_z are, respectively, the characteristic horizontal and vertical scales and velocities. To the lowest order in δ one finds that the pressure deviation $p = P - P_H$ from the hydrostatic equilibrium $P_H = \rho_0 g^* H_0(1-z)$ is independent of the depth. Then, from the Euler equations and the boundary conditions one obtains the standard equations for a rotating shallow-water layer with a free surface (Pedlosky 1987):

$$\mathrm{D}_t \boldsymbol{V} + f\boldsymbol{k} \times \boldsymbol{V} = -\frac{1}{\rho_0}\boldsymbol{\nabla} p, \tag{1}$$

$$p = \rho_0 g^* \Delta h, \tag{2}$$

$$\mathrm{D}_t H + H(\boldsymbol{\nabla} \cdot \boldsymbol{V}) = 0, \tag{3}$$

where $\mathrm{D}_t = \partial_t + \boldsymbol{V} \cdot \boldsymbol{\nabla}$, Δh is the deviation of the free surface, H is the total height of the layer $H = H_0 + \Delta h$, V is the horizontal velocity and $\boldsymbol{k}$ is the normal unit vector aligned with the effective gravity g^* which, in the paraboloidal experiment, includes gravitational and centrifugal accelerations (see figure 1).

The beta-plane approximation consists of taking a linear term in the expansion of the normal component Ω_z of the angular velocity at some constant colatitude θ:

$$f = 2\Omega_z = f_0(1 + \beta y), \tag{4}$$

where y is the dimensionless meridional coordinate directed towards the centre of the vessel, f_0 is the local Coriolis parameter

$$f_0 = 2\Omega_0 \cos\theta \tag{5}$$

and β characterizes the variation of Ω_z with latitude ('beta-effect'). Note that f_0 decreases when the paraboloidal colatitude θ increases (see figure 1); the 'north' is therefore located at the centre of the vessel. A northward (southward) direction is a direction towards (away from) the centre. As mentioned in the Introduction, in the paraboloidal geometry the effective gravity g^* also has a latitude dependence, unlike the planetary case. Therefore

$$g^* = \frac{g}{\cos\theta}(1-\beta y). \tag{6}$$

The specific beta-parameter for the paraboloidal geometry is given by

$$\beta = -\frac{L_0}{R_c f_0}\frac{\partial f}{\partial \theta} = L_0\frac{\Omega_0}{g}\cos^2\theta\sin\theta, \tag{7}$$

where $R_c = g/(\Omega_0^2\cos^3\theta)$ is the local curvature of the paraboloidal free surface. β should be small ($L_0 \ll R_c$) in order to justify the beta-plane approximation. Note that β vanishes at the centre of the paraboloid $\theta = 0$ while it is maximum at $\theta \approx 35°$.

According to the geostrophic balance assumption the pressure gradient is compensated by the Coriolis force at the first order of approximation. The geostrophic balance is then satisfied if we can neglect in (1) the inertial terms in comparison with the Coriolis terms. In order to estimate the ratio of these two terms the dimensionless Rossby number is introduced:

$$\epsilon = \frac{V_0}{L_0 f_0} = \frac{T_0}{2T_{int}\cos\theta}, \tag{8}$$

where T_0 is the period of rotation of the vessel and T_{int} the characteristic internal rotation in the core of the vortex.

We also define a dimensionless relative elevation parameter which characterizes the amplitude of the vortex:

$$\lambda = \Delta h/H_0, \tag{9}$$

where Δh is the deviation of the free surface from the hydrostatic equilibrium at the centre of the vortex. For vortices in geostrophic balance ($\epsilon \ll 1$) we get, according to (1) and (2), a simple scaling relation between λ and the Burgers number Bu:

$$\lambda = \epsilon\left(\frac{L_0}{R_{Rossby}}\right)^2 = \frac{\epsilon}{Bu}, \tag{10}$$

where we introduce the local Rossby radius:

$$R_{Rossby} = \frac{(g^* H_0)^{1/2}}{f_0} = \frac{(gH_0)^{1/2}}{2\Omega_0\cos^{3/2}\theta}. \tag{11}$$

We deliberately chose to characterize the vortex by λ rather than Bu^{-1} because, according to our depth measurement technique (see below) we directly measure λ and the dispersion of results is, thus, reduced.

The set of equations (1), (2) and (3) admits dispersive Rossby wave solutions. On the infinite beta-plane tangent to the paraboloid (cf. Nycander 1993; Stegner & Zeitlin 1995) at the lowest order in ϵ, β one gets a well-known relation for these waves:

$$\omega = -V_{Rossby}\frac{k_x}{1+R_{Rossby}^2(k_x^2+k_y^2)}, \tag{12}$$

where

$$V_{Rossby} = R_{Rossby}^2\frac{1}{R_c}\frac{\partial f}{\partial\theta} = \tfrac{1}{2}\Omega_0 H_0\sin\theta \tag{13}$$

is the maximum westward phase speed of linear Rossby waves. Relation (13) does not take into account the possible topographic effects (gradients in the thickness of the unperturbed layer H_0) which may play an important role in paraboloidal geometry. Nevertheless, it is possible, by using an accurately adjusted rotation Ω_0 to eliminate such topographic effects at a given latitude. We deliberately restrict our study to this case.

No dissipation was introduced in (1)–(3). However, as far as the experiment is concerned, the effects of the viscous boundary (Ekman) layer at the bottom of the vessel play an important role. At the lowest order the Ekman layer affects the dispersion relation of the Rossby waves as follows (Pedlosky 1987):

$$\omega = -V_{Rossby}\frac{k_x}{1+R_{Rossby}^2(k_x^2+k_y^2)} - \mathrm{i}\frac{R_{Rossby}^2(k_x^2+k_y^2)}{1+R_{Rossby}^2(k_x^2+k_y^2)}\frac{1}{2T_E}, \tag{14}$$

where T_E is the standard Ekman spin-down time:

$$T_E = \frac{H_0}{(\nu f_0)^{1/2}}. \tag{15}$$

According to (14), the decay rate of a localized linear Rossby wave packet is scale-dependent. Hence, in the framework of the linear analysis, we get from (14) a characteristic spin-down time

$$T_{spin\text{-}down} = 2\left(\frac{L_0}{R_{Rossby}}\right)^2\left[1+\left(\frac{R_{Rossby}}{L_0}\right)^2\right]T_E \tag{16}$$

for an isolated vortex of characteristic scale L_0.

Note that like the Rossby radius, the Rossby velocity V_{Rossby} and the Ekman time T_E depend only on the parameters of the unperturbed layer and are not sensitive to the size and velocities of the vortex perturbation. We therefore use these parameters to rescale data obtained in different unperturbed layers.

3. Experimental procedure

In the paraboloidal geometry the beta-effect is due to the latitude dependence of the local normal component of rotation Ω_z, exactly like in a spherical planetary shallow-water layer. However, in order to neglect the effect of the horizontal component Ω_y a condition $\delta = H_0/L_0 \ll 1$ should be strictly satisfied. In order to fulfil this condition we used a thin layer in all of our experiments and, therefore, the thickness parameter δ was in the range 0.05–0.25. This condition is more stringent than for the experiments with a flat layer of slowly rotating fluid where the vertical angular velocity Ω_z is constant throughout the layer. In this latter case the 'horizontal Coriolis effect' is absent and the shallow-water approximation ensuring two-dimensionality of the flow is still valid if $\delta \approx 1$ as long as the Rossby number remains small.

3.1. *The experimental setup*

Figure 2 shows a schematic side view of the experimental apparatus. The fluid layer lines a parabolic Plexiglas vessel of shape $z = pr^2$ with $p = 2.67\ \mathrm{m}^{-1}$ and 45 cm in diameter.

A system of twelve halogen lamps is mounted around the vessel and a conical

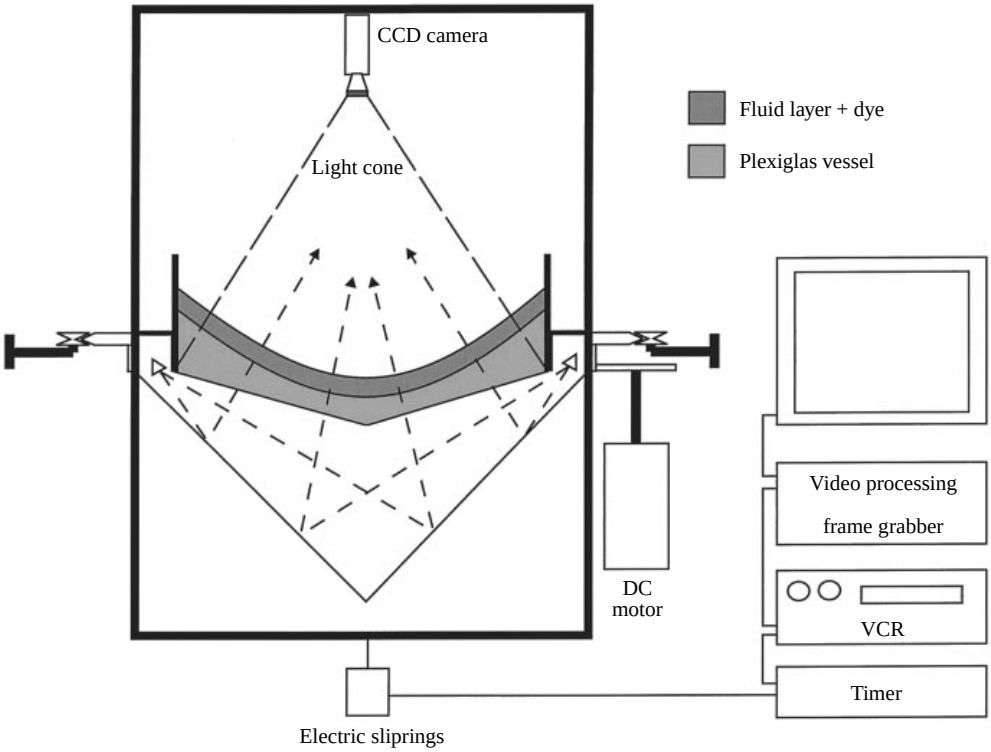

FIGURE 2. Sketch of the experimental apparatus.

reflector is used to obtain practically homogeneous lighting of the fluid layer from below through the transparent Plexiglas vessel. The image of the fluid layer is taken by a sensitive black-and-white CCD camera (Hitachi KP-M1) mounted on the rotating frame. We use a wide-angle lens and fix the camera close to the vessel in order to reduce the geometrical distortion of the image due to the parabolic shape of the fluid layer. The video signal passes through an electric slipring (Air Precision T13SD) to be recorded by a high-resolution VCR (Panasonic AG-7355 S-VHS). Since the video signal is the only AC signal passing through the sliprings, there are no 'diaphonic' mixing or perturbations whatsoever.

The rotating cell containing the paraboloidal vessel, the lighting system, the video camera and a small injection-suction system (see below), is driven by a DC servomotor (CEM T5F2C). Note that this motor is not fixed on the axis of rotation of the apparatus (unlike classical turntables). The whole rotating cell is mounted inside a large ring which is supported by three wheels. A gearing connects the motor to the ring. The rotation of the whole system is controlled by an optical encoder yielding 26 500 counts for one revolution of the vessel. The main rotation rate (70.98 r.p.m. for a fluid layer of 12 mm) was observed to be stable with an accuracy of 0.1 %.

3.2. *Measurement techniques*

The main idea of this technique is to measure the height of the fluid layer from the light absorption in the uniformly dyed water. The dye used in experiments (Amaranth) has a maximum absorption rate at 520 nm wavelength. Therefore, to improve the sensitivity of the system we put a specific pass-band filter on the video camera, in order to select visible light in a narrow band between 480 and 560 nm. The video camera

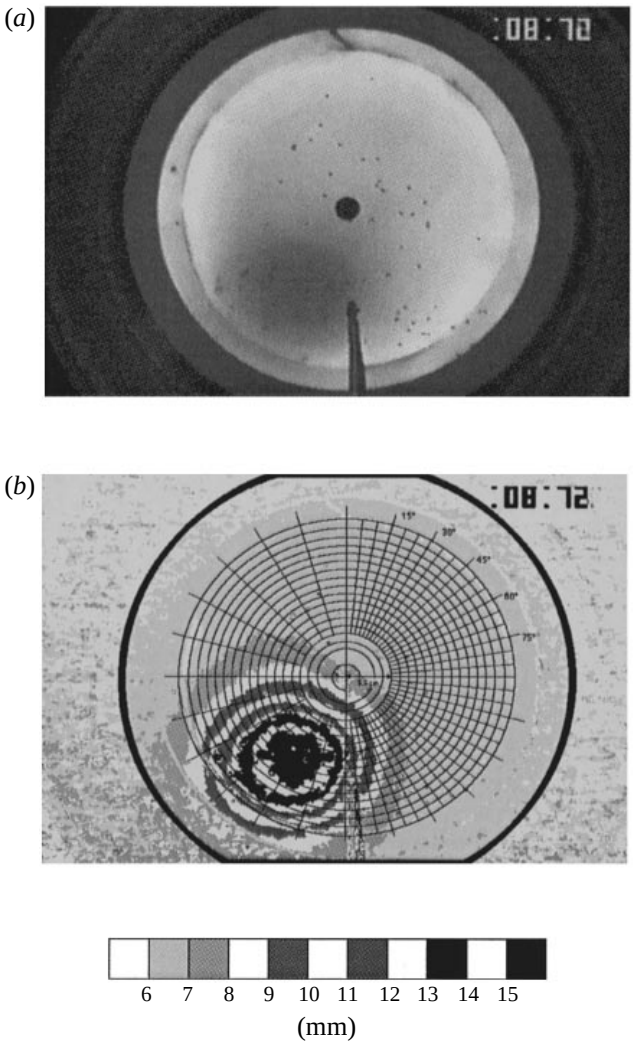

FIGURE 3. (*a*) Camera image and (*b*) the topographic map of the free surface resulting from the video processing of a large-scale anticyclone generated by injection; the dark circle in (*b*) indicates the actual location of the sidewall boundary; the characteristic vortex size, as defined below, corresponds, roughly, to 11 mm level.

output is digitized in a frame of 768×512 pixels with a resolution of 256 grey levels by means of a frame grabber and image processing software (NIH 1.55 for Macintosh). In the final black-and-white digitized camera image the pixel intensities depend linearly on the light intensity after absorption in the fluid layer. Hence, for a local elevation of the free surface the light absorption will be higher and this region will appear dark on the video image (see figure 3*a*). The inverse exponential relation between the pixel intensity and the layer thickness according to the Beer–Lambert law of absorption was carefully checked. In order to have an accurate calibration, which would take into account the deviation of the light intensity from perfect uniformity, several reference images (15 to 25) of different thickness were recorded. These reference images correspond to unperturbed fluid layers at hydrostatic equilibrium having constant thickness.

Starting from a black-and-white camera image (figure 3*a*) we construct a topographic map of the free surface using either shading (figures 3*b*, 16) or false colours (figures 8 and 9), each change in shading/colour corresponding to a depth variation of 1 mm. Besides, a small region (5×5 pixels) on this image could be selected and a specific grey-level averaging process applied to get a more precise measurement of the local mean thickness. To check the calibration and estimate the accuracy of the height measurements we recorded images of the unperturbed fluid layer with several rectangular pieces of glass of a known thickness put at the bottom of the tank. We therefore created local changes in the thickness of the fluid layer. These relative depth variations were detected by the thickness measurement procedure with an accuracy of 5%. In addition, in order to estimate the caustic effects, we fixed a thin curved glass at the bottom of the tank which trapped an air lens and, thus, mimicked a smooth circular dip of the free surface. The focusing or defocusing of light beams due to the curvature of the air–fluid interface may introduce a systematic amplification or attenuation of the light intensity independent of the dye absorption. The systematic error due to this caustic effect was observed to be less than 8%, for the strongest curvature. We therefore estimate that the errors of the height measurement technique we used do not exceed 10%. We should emphasize that no height measurement can be made close to the boundary of the vessel, as the light cone (see figure 2) does not cover the whole surface of the fluid layer. Consequently, our topographic map pictures do not represent the fluid layer as a whole. The dark circle in figure 3(*b*) shows the location of the real sidewall boundary.

Together with these altimetric measurements, we use, when necessary, streak particle velocimetry and colour-dye visualization.

3.3. *Generation of vortices*

As mentioned in §2, the fast rotation of the vessel produces a flow in geostrophic balance. The velocity field follows the isobars. Hence, if a region of high pressure (elevation) is created locally an anticyclonic circulation will appear and, inversely, for a low-pressure region (dip) a cyclonic circulation results. Among several methods we have tested, the injection or suction techniques appears to be the best for the generation of isolated and almost circular vortices. To obtain an anticyclone we inject a small amount of fluid from above the unperturbed layer, as shown in figure 4(*a*). To get large-scale cyclones a thin disk of 4 cm diameter (see figure 4*b*) is fixed at the end of the pipe (diameter 8 mm) to increase the suction section. We introduce this device in the unperturbed layer and we remove the pipe from the layer immediately suction is over. The volume of the injected or sucked liquid varied from 50 ml to 300 ml with a mean flow rate of $35\ \mathrm{ml\ s^{-1}}$. Note that the mechanical pumping used in our experiments did not allow a significant change of the flow rate.

During the generation process, when the local thickness of the layer varies rapidly, a strong chaotic and three-dimensional motion occurs. However, after a rapid period of geostrophic adjustment a vortex obtained from this perturbation becomes quasi-axisymmetric and respects the geostrophic balance. All the values of the dimensionless parameters λ, ϵ, β given in this paper are measured in this initial state, just after the adjustment process, a few seconds after the injection or suction has been stopped.

The measured Rossby numbers for vortices produced in this way are small (although not infinitesimally small), which confirms the basic geostrophic balance hypothesis. In figures 5(*a*) and 5(*b*) we give some typical examples of the radial azimuthal velocity profiles for an anticyclone and a cyclone which we get from particle-streak velocimetry. The Rossby numbers are $\epsilon = 0.23$ and 0.13, respectively. It is clear that the structures

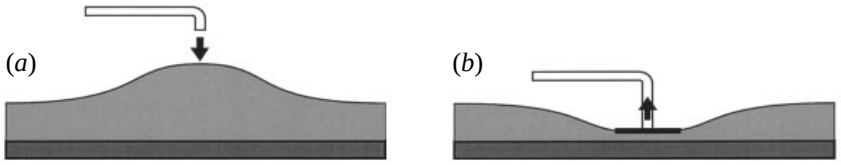

FIGURE 4. Generation of quasi-axisymmetric vortices in geostrophic balance: (*a*) injection to produce an anticyclone; (*b*) suction with a pipe with attached disk to get a large-scale cyclone.

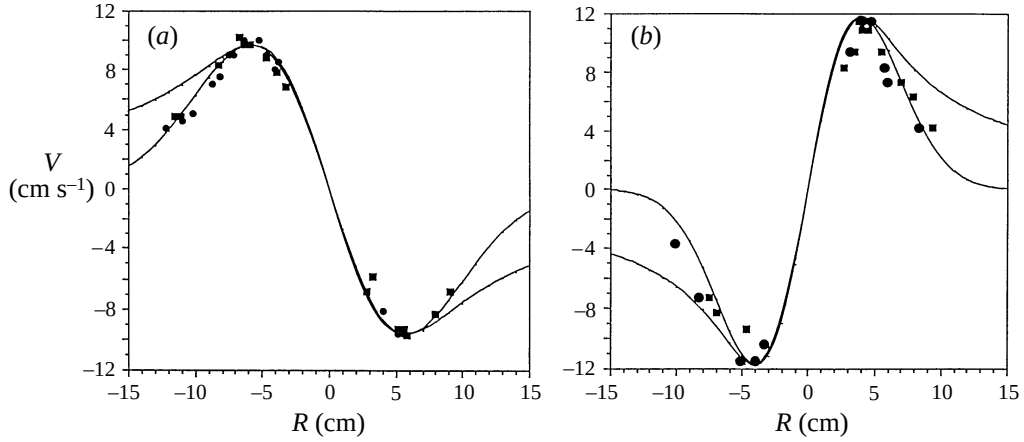

FIGURE 5. Radial distribution of azimuthal velocity for a typical (*a*) anticyclone, (*b*) cyclone. Circles (squares) correspond to the x-(y-) component of the azimuthal velocity. Exponential (isolated vortex) and $1/r$ (non-isolated vortex) fits are also plotted.

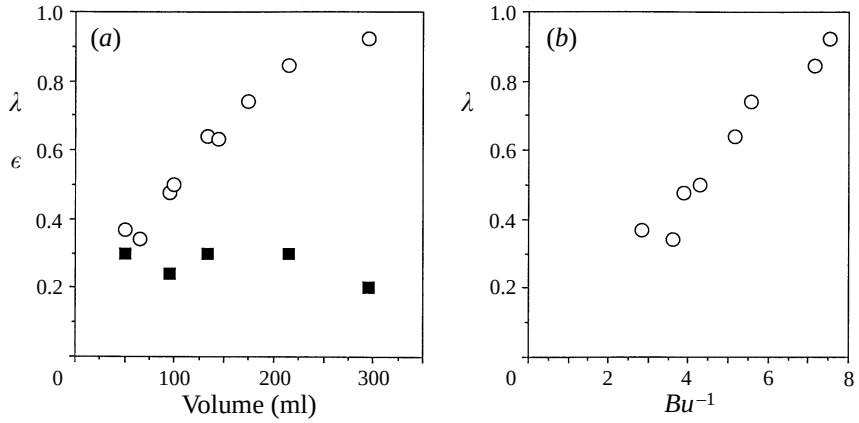

FIGURE 6. Characteristic parameters of anticyclones obtained with different volume of injection in the same unperturbed layer of thickness $H_0 = 11{,}.5$ mm: (*a*) relative elevation parameter λ (open circles) and Rossby number ϵ (filled squares) as functions of the injected volume (*b*) dependence of λ on $Bu^{-1} = (L_0/(R_{Rossby})^2$.

obtained are indeed isolated in the sense that their velocity decays faster than $1/r$. In other words, the circulation vanishes outside the vortex. We pay special attention to this point because of the fact that non-isolated structures were being produced by the suction method in some previous studies (Carnevale *et al.* 1991).

We have also observed that when we increased the amount of injected liquid in the unperturbed layer of thickness $H_0 = 11.5$ mm the relative elevation and size of the

vortex increased whereas its Rossby number remained small (see figure 6*a*). The relation between the size and the relative elevation of the resulting vortices is presented in figure 6(*b*). We see that the relation between λ and Bu^{-1} at an almost constant Rossby number is linear, in agreement with equation (10) where the characteristic scale L_0 is defined as half of the relative elevation radius $h(r = L_0) = H_0 + \frac{1}{2}\Delta h_{max}$. Similar results were also obtained for anticyclones with $H_0 = 6$ mm. These observations confirm that the vortex motion respects the geostrophic balance and, thus, the basic idea of the intermediate models.

4. Results

In all our experiments the Rossby number and the dimensionless beta-parameter were observed to be of the same order: $\beta \approx 0.1$ and $\epsilon \approx 0.1$–0.3. By changing the thickness of the unperturbed layer (4 to 24 mm) we were able to vary the Rossby radius from 1.4 to 3.5 cm and by changing the volume perturbation we get vortices with characteristic radius L_0 from 4.5 to 7.5 cm. In this way we got quantitative results for vortices with the relative elevation parameter λ in the range from 0.25 to 3.5 and the characteristic horizontal scale L_0 from $L_0 = 0.8R_{Rossby}$ to $L_0 = 4.2R_{Rossby}$.

4.1. *Quasi-geostrophic versus nonlinear dynamics*

Figure 7 shows the evolution of a passive tracer for two different anticyclonic vortices. In this experiment, the unperturbed water layer contains no dye, while the volume injected has a strong dye concentration. The volume injected, the flow rate and the location of the pipe are identical for the two cases. The only difference is the thickness of the unperturbed layer, 24 mm for figure 7(*a*) and 6 mm for figure 7(*b*). We therefore have a small relative elevation in the first case and a strong one in the second case. For the small relative elevation (estimated to be 0.25) the fluid in the outer shear region surrounding the strong central anticyclone is peeled off the structure and cast aside. A cyclonic dye pattern emerged from this shear region. Besides, we notice that while the central anticyclone drifts westwards, there is also a non-negligible meridional southward drift. These dynamical properties are close to the behaviour of relatively small-scale ($L_0 < R_{Rossby}$) vortices propagating on the topographic beta-plane (Carnevale *et al.* 1991). Note that the evolution of the dye concentration in an isolated cyclone shown by these authors (figure 4 in their paper) has a striking similarity with our results. On the other hand, for a strong relative elevation (estimated to be 1.3) the coherence and the longevity of the anticyclone are much more pronounced. The dye pattern stays circular and drifts westwards at a constant latitude with almost no southward deviation. These results indicate that two qualitatively different dynamical regimes are possible in the framework of the paraboloidal experiment.

To confirm this observation we used the height measurement procedure described above and allowing a fully quantitative analysis. Figure 8 shows the time evolution of the free surface represented by the topographic maps in false colours for an anticyclone generated at the same conditions as the vortex shown in figure 7(*a*). As expected, the initial relative elevation λ at the centre of the anticyclone is small, $\lambda = 0.25$, and is of the same order as the Rossby number. The initially axisymmetric anticyclone quickly loses its symmetry while a cyclonic tail appears and increases in amplitude. The centre of the anticyclone (the point of maximum amplitude) drifts southwestwards. This kind of behaviour is typical of an isolated barotropic vortex in the standard QG regime where $\lambda \approx \epsilon \approx \beta$. Indeed, laboratory (Firing & Beardsley 1976; Masuda *et al.* 1990; Carnevale *et al.* 1991), numerical (McWilliams & Flierl 1979; Mied & Lindemann

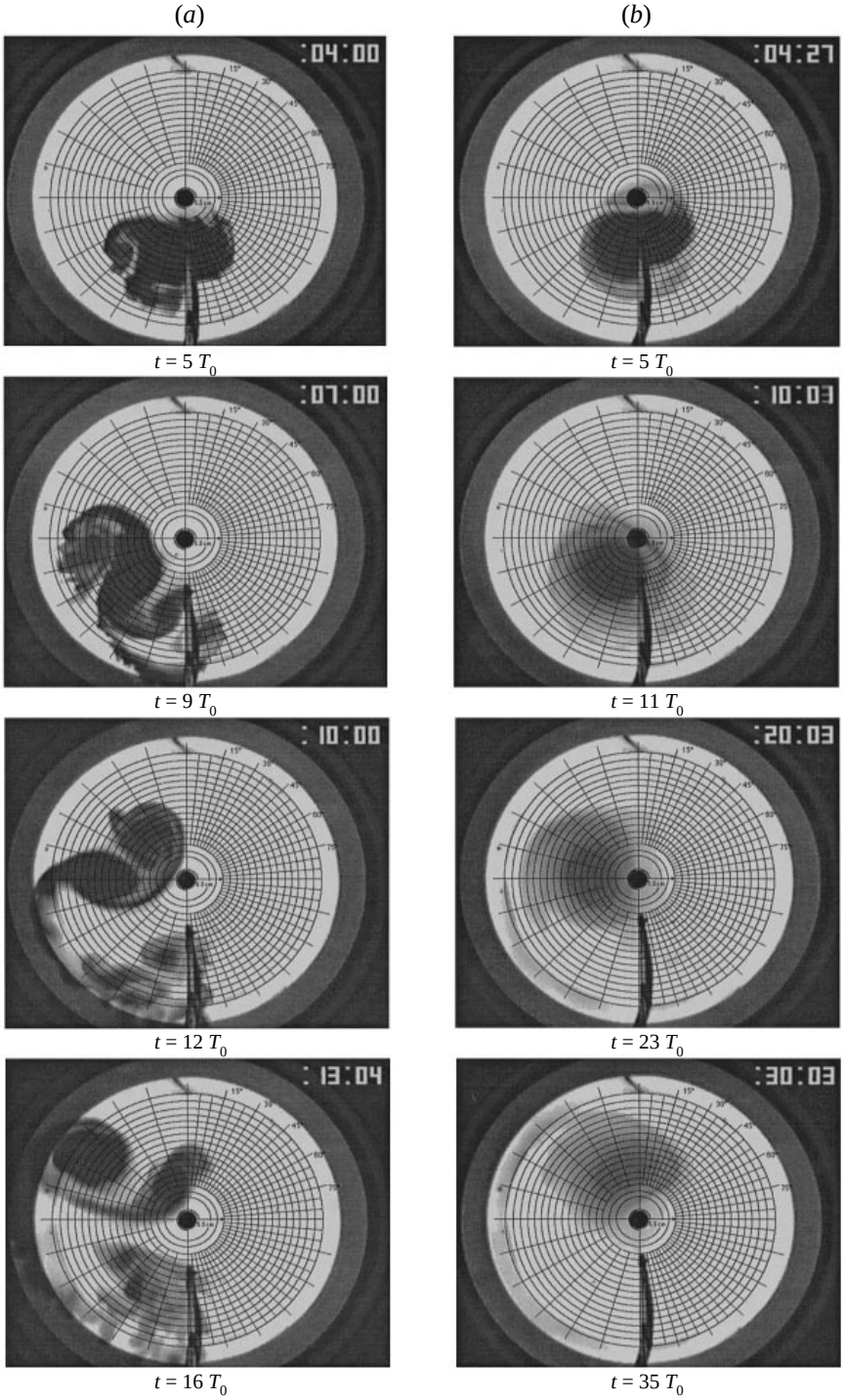

FIGURE 7. Dynamical evolution of an anticyclonic vortex for (*a*) small ($\lambda \approx 0.25$) and (*b*) high ($\lambda \approx 1.3$) relative elevation. The volume injected into the unperturbed pure water layer contains a strong concentration of dye. The injected volume (135 ml), the flow rate and the location of the pipe are strictly identical for the two cases. The thickness of the unperturbed layer is (*a*) $H_0 = 24$ mm and (*b*) $H_0 = 6$ mm; the period of rotation of the vessel is (*a*) $T_0 = 0.821$ s; (*b*) $T_0 = 0.856$ s.

1979; Sutyrin *et al*. 1994) and theoretical investigations (Sutyrin & Flierl 1994; Reznik & Dewar 1994) have clearly established the tendency for a QG anticyclone (cyclone) to propagate to the southwest (northwest). Besides, owing to the Rossby wave dispersion the initial vortex leaves a Rossby wave wake behind it and develops a wavenumber 1 axial asymmetry. This fact was carefully checked in numerical simulations of McWilliams & Flierl (1979) and Mied & Lindemann (1979), and the experiment of Firing & Beardsley (1976). Therefore, the appearance of an increasing circulation of opposite sign behind the initial vortex can be seen as a signature of a Rossby wave wake.

The evolution of a nonlinear anticyclone generated at the same conditions as in figure 7(*b*) is shown in figure 9. We observe here a strong elevation ($\lambda = 1.3$) and large-scale ($L_0 = 3.7R_{Rossby}$) vortex. As in figure 7(*b*) the anticyclone remains circular and propagates westwards with no meridional drift. Besides, we note that unlike the case of the QG anticyclone described above there is no evidence of any cyclonic circulation behind the main vortex. In order to determine the range of the parameter λ where these large-scale and long-lived vortices can be obtained we generated numerous anticyclones and studied systematically their lifetimes and drift velocities.

Let us add that, although we cannot prove this rigorously, we do not think that the sidewalls effects play a significant role in selecting the pattern of vortex behaviour. Indeed, the geometry of the initial configuration and the absolute vortex radius do not change much from, say, figure 8 to figure 9 (let us recall that it is the ratio of the vortex radius to the Rossby radius which determines the dynamical regime and not the radius itself). Quantitatively, the geometric parameter (vortex radius)/(distance from the wall to the vortex centre) is approximately the same (0.3 and 0.4, respectively). Hence, *a priori*, the influence of the boundaries is roughly the same in the two cases while the vortex behaviour is completely different. The main difference comes from the characteristics of the unperturbed shallow-water layer: $H_0 = 24$ mm, $R_{Rossby} = 3.5$ cm for figure 8 and $H_0 = 6$ mm, $R_{Rossby} = 1.8$ cm for figure 9. Hence, it is the relative elevation parameter λ which governs the transition between the two dynamical regimes.

4.2. *The influence of the Ekman spin-down mechanism and Rossby wave dispersion on the lifetime of anticyclones*

One may observe in figure 9 that while an anticyclone drifts at a constant latitude it spreads symmetrically and its amplitude slowly decreases. We plot its relative elevation as a function of time on figure 10. This evolution is properly fitted by an exponential decay and we, therefore, define a characteristic lifetime T_{life} for each vortex as its e-fold decay time.

As already mentioned in §2, the Ekman layer plays an important role in the experiment. Indeed, the Ekman spin-down is rapid even for small Ekman numbers E_k. For the present experiment the value of $E_k = \nu/(2\Omega_0 H_0^2 \cos\theta)$ is about 10^{-3} and the characteristic thickness of the Ekman boundary layer $d_E = (\nu/\Omega_z) \approx 0.3$ mm, with $\nu = 10^{-6}$ m^2 s^{-1} for the kinematic viscosity of water. The main problem arising when studying vortex lifetimes is to separate the contribution of the Ekman spin-down from that of the Rossby wave dispersion/emission process. Therefore, we decided to measure the lifetimes of anticyclones drifting at $\theta \cong 30°$ where the beta-effect is maximal and compare them with the lifetimes of anticyclones generated at the centre of the vessel, where there is basically no beta-effect (the *f*-plane situation). In this latter case the lifetimes are expected to be entirely determined by the Ekman spin-down. We use the Ekman spin-down time (Pedlosky 1987) based on the quasi-geostrophic

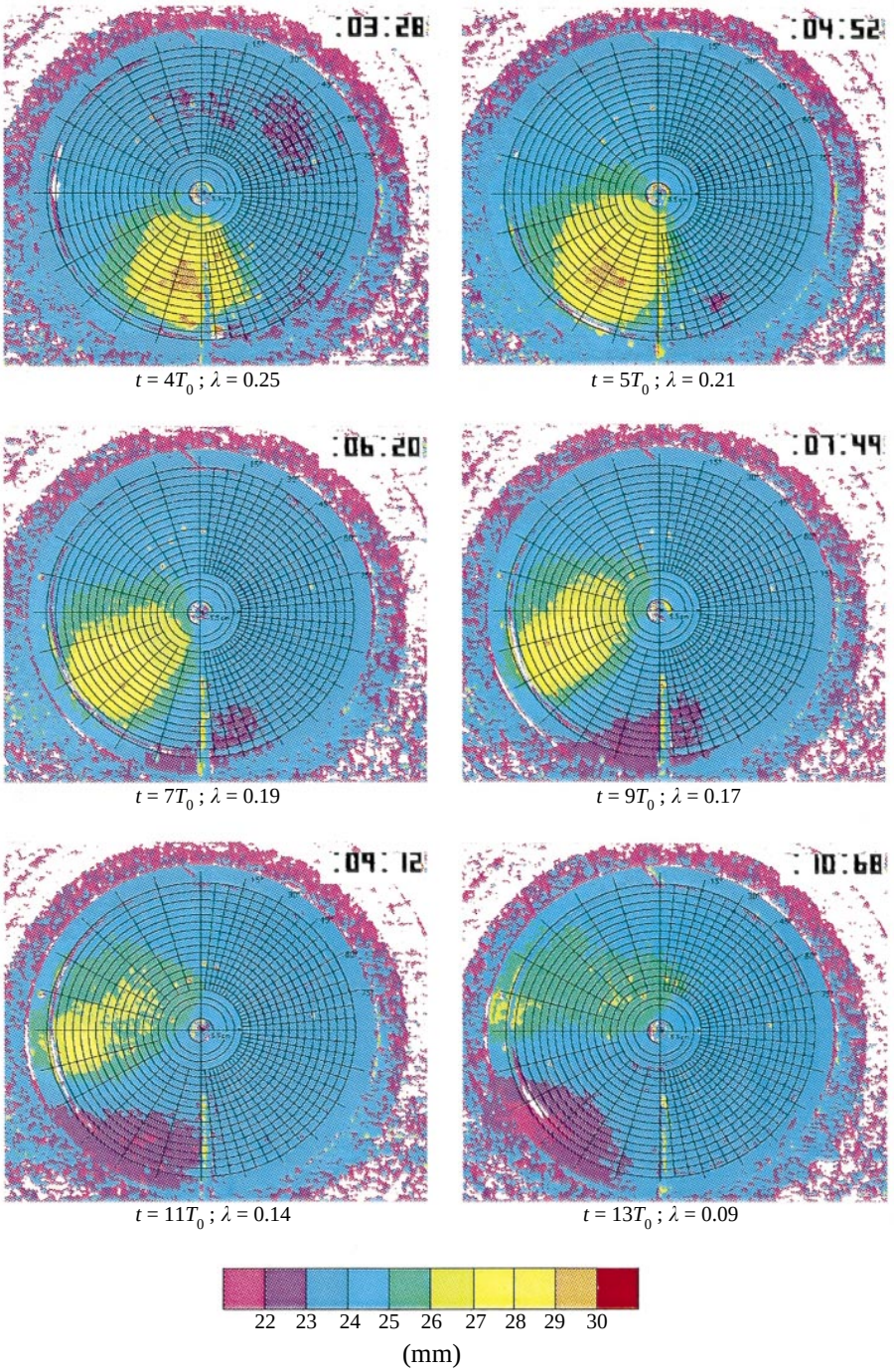

FIGURE 8. Topographic maps of the free surface for a quasi-geostrophic anticyclone. The injected volume (140 ml), the flow rate, the thickness of the unperturbed layer ($H_0 = 24$ mm) and $T_0 = 0.821$ s are the same as in figure 7 (*a*). The characteristic horizontal scale $L_0 = 4.5$ cm is of the same order as the Rossby radius $R_{Rossby} = 3.5$ cm.

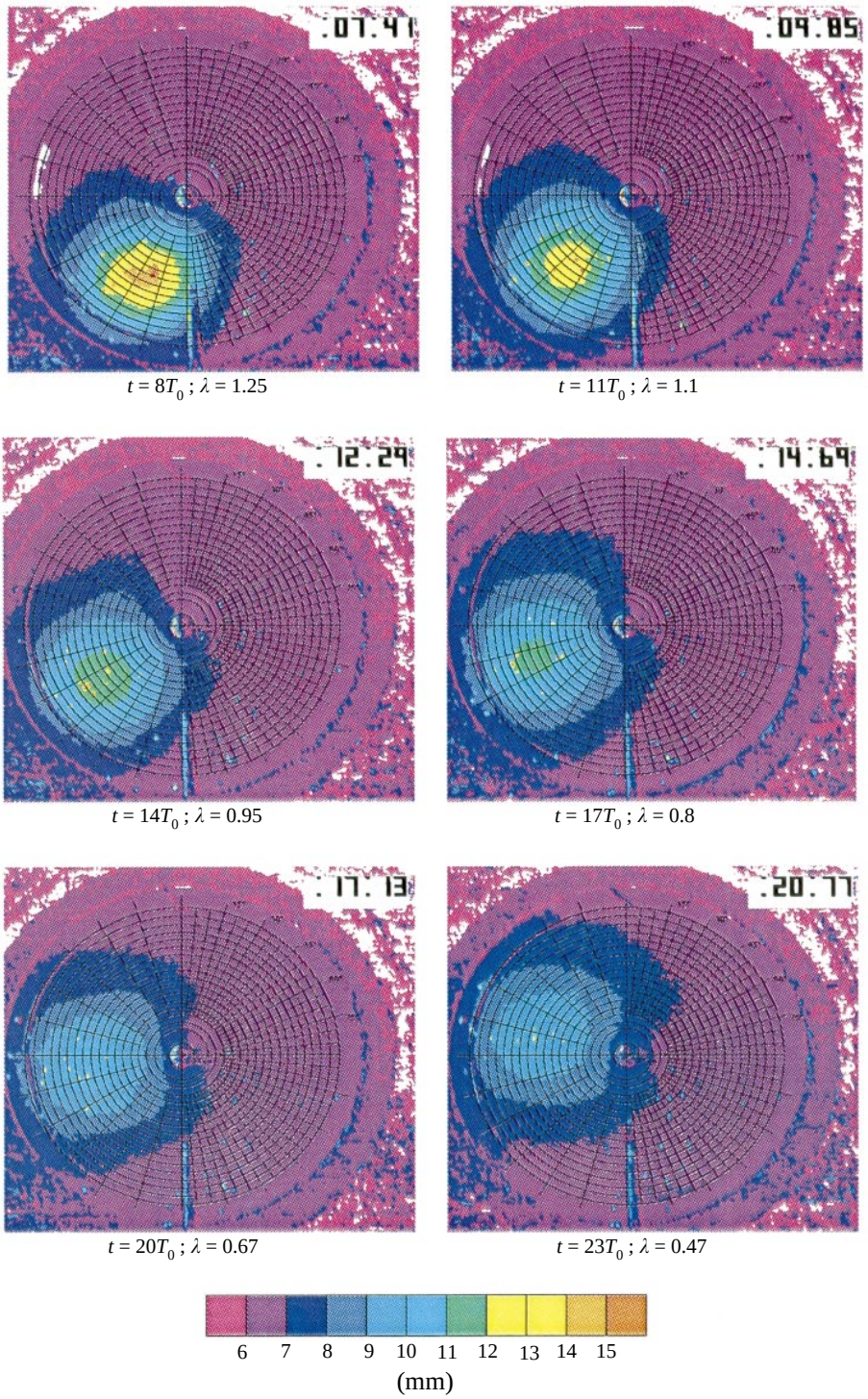

FIGURE 9. Topographic maps of the free surface for a strongly nonlinear anticyclone. The injected volume (140 ml), the flow rate, the thickness of the unperturbed layer ($H_0 = 6$ mm) and $T_0 = 0.856$ s are the same as in figure 7(*b*). The characteristic horizontal scale $L_0 = 6.5$ cm is larger than the Rossby radius $R_{Rossby} = 1.8$ cm.

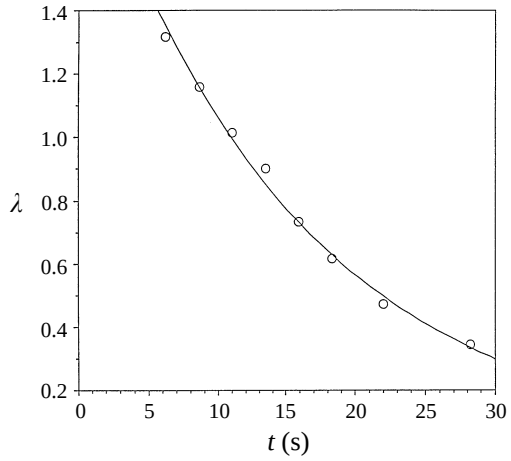

FIGURE 10. Relative elevation λ of the large-scale anticyclone of figure 9 as a function of time. Solid line represents an exponential decay fit. The characteristic lifetime is $T_{life} = 15.7$ s $\approx 18T_0$, while the internal period of rotation is $T_{int} \approx 2$ s at the initial state.

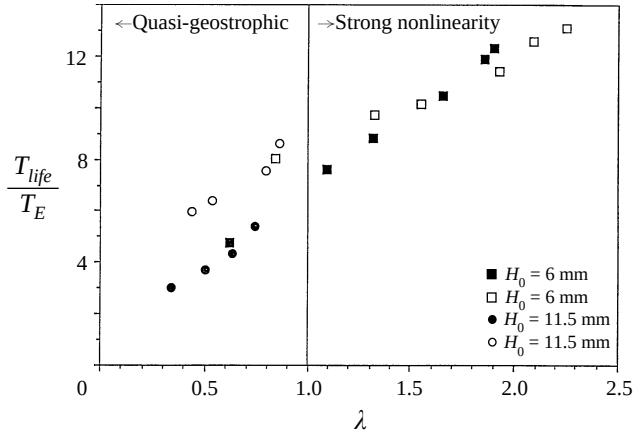

FIGURE 11. Lifetimes of anticyclones rescaled by the standard Ekman spin-down time (15), as a function of the relative elevation parameter λ. Open symbols correspond to the vortices generated at the centre (no beta-effect), filled symbols represent vortices generated at $\theta = 30°$ (maximum beta-effect).

estimates to rescale the data obtained with different thicknesses H_0 of the unperturbed layer. The results of this analysis are presented in figure 11.

The open symbols in figure 11 represent the anticyclones generated at the centre and, thus, give an idea how the Ekman spin-down affects the lifetime of vortices. We first note that the lifetimes increase linearly with the relative elevation of the vortices. If we take into account the observed relation between λ and Bu described in figure 6(b) and discussed previously in §3.3, we see that the linear dependence of the lifetime on λ is in agreement with the relation (16). Besides, when the vortices tend to the quasi-geostrophic regime, $\lambda \approx \epsilon \ll 1$, $L_0 \approx R_{Rossby}$, we note that $T_{life} \sim 4T_E$ which is also in surprisingly good agreement with (16). However, the slope of the linear dependence of T_{life} on λ is overestimated by (16) which is, probably, a signature of the nonlinear effects in the Ekman mechanism for strong relative elevations.

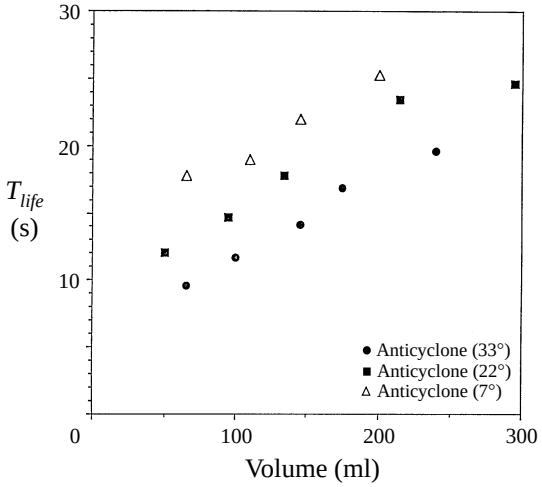

FIGURE 12. Lifetimes of anticyclones as a function of injected volume. Relative elevations are within the range 0.4–0.9. Vortices are generated at three different colatitudes: 7°, 22° and 33° in the same unperturbed fluid layer $H_0 = 11.5$ mm.

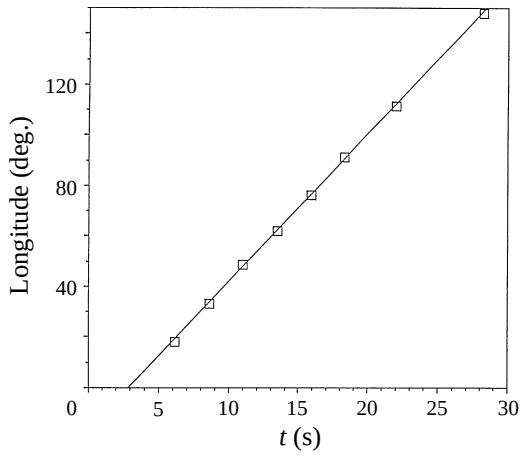

FIGURE 13. Subsequent longitudinal angular positions of the vortex centre (extremum of elevation) as a function of time for the strongly nonlinear anticyclone of figure 9. Solid line represents a linear fit with a constant angular westward drift velocity of 5.8° s^{-1}.

The influence of the Rossby wave dispersion on the lifetime can be deduced from the comparison of the open circles with the filled ones in figure 11. We can clearly see that for small relative elevations ($\lambda < 0.5$): $T_{life(centre)} \approx 2T_{life(30°)}$. In this regime close to the quasi-geostrophic scales the lifetimes of anticyclones drifting at $\theta \approx 30°$ are reduced by the Rossby wave dispersion. This result is confirmed by the analysis of the corresponding topographic maps of the free surface which exhibit a very weak dip (cyclonic circulation) behind the main elevation (anticyclonic vortex). We plot in figure 12 the measured lifetime as a function of the injected volume for several anticyclones ($0.3 < \lambda < 0.8$) generated at different colatitudes in the same unperturbed layer of thickness $H_0 = 11.5$ mm. Here, again, the lifetime of the vortex of a given size decreases when its beta-parameter increases. On the other hand, for strong relative elevations ($\lambda > 1$) we find that $T_{life(centre)} \approx T_{life(30°)}$, i.e. the lifetimes of vortices are determined

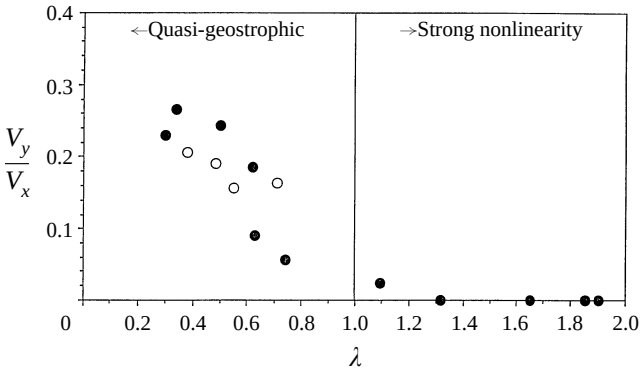

FIGURE 14. Ratio (in the absolute values) of the meridional drift velocity V_y and the westward drift velocity V_x. Filled circles correspond to anticyclones, open circles to cyclones.

entirely by the Ekman spin-down mechanism. Hence, for the nonlinear anticyclones with $\lambda > 1$ the lifetimes seem not to be affected by the Rossby waves dispersion.

4.3. *Analysis of drift velocities*

In order to measure the westward drift velocity, we plot the longitudinal angular position of the vortex centre (extremum of elevation) as a function of time. We show in figure 13 a plot corresponding to the large-scale anticyclone of figure 9. All the points fit a straight line, from which we deduce the angular drift velocity of the vortex. Hence, although the amplitude of the vortex decreases with time (see figure 9), the drift velocity remains perfectly constant. However, as we have seen before, a vortex may have a meridional drift in addition to the mean westward propagation. We thus plot in figure 14 the absolute value of the ratio of the meridional drift velocity V_y and the westward drift velocity V_x. These quantitative measurements confirm the qualitative observations of §4.1. The meridional propagation due to a weak asymmetric circulation is typical of quasi-geostrophic vortices, while for vortices with strongly nonlinear dynamics ($\lambda > 1$) the meridional drift component V_y vanishes.

According to previous experimental results obtained with a paraboloidal vessel in the case of forced monopolar vortices in a thin shallow-water layer (Rasmussen, Stenum & Snezhkin 1996) and in the case of free isolated vortices in a thick layer (Nezlin *et al.* 1996) the drift velocity of a vortex depends both on its amplitude and the characteristics of the unperturbed layer. This latter is generally characterized by the maximum westward phase speed of the linear Rossby waves for the infinite beta-plane locally tangent to the shallow-water layer at a given latitude. In order to investigate the dependence of the drift velocity on vortex amplitude and to compare our experimental results with the predictions of the centre-of-mass argument of Nycander (1993) we plot in figure 15 the drift velocity non-dimensionalized by the Rossby velocity (13) as well as the value given by Nycander's formula.† We first note that for a given depth the dependence of the westward drift velocity on λ is weak, as predicted by Nycander's formula. But on the other hand, a disturbing feature of this graph is that the results for

† In order to calculate the dimensionless integrals in Nycander's formula

$$V_x = -V_{Rossby}\left[1+\lambda(R_{Rossby}/L_0)\int(1+\lambda h)\,h_x^2\,\mathrm{d}x\,\mathrm{d}y\left(\int h\,\mathrm{d}x\,\mathrm{d}y\right)^{-1}\right]$$

written here in the absence of topography (which is our case), we approximate the experimental vortices by the Gaussian shape $h(x,y) = \exp((x^2+y^2)/1.44)$.

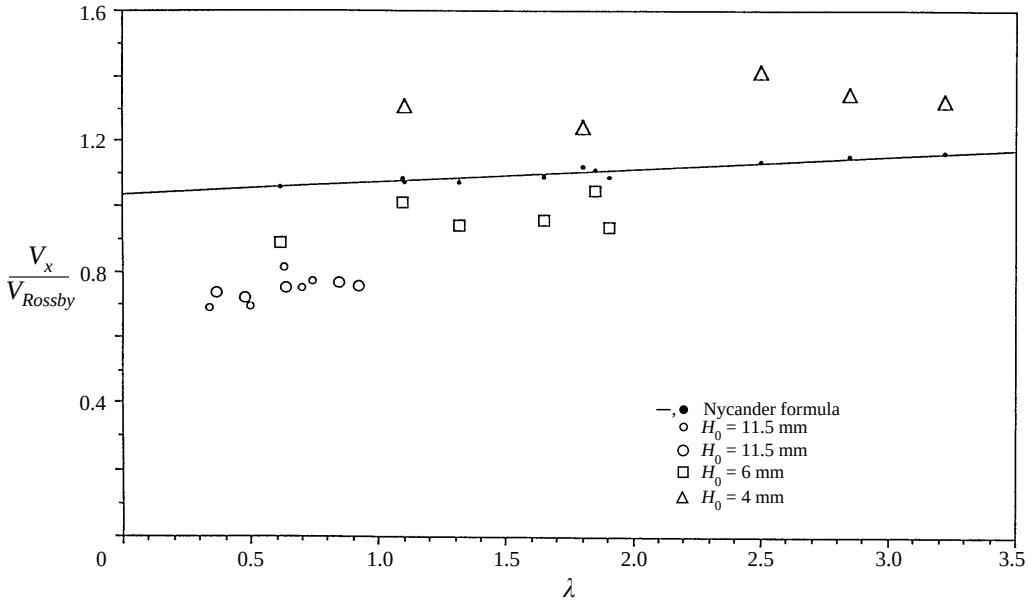

FIGURE 15. Ratio V_x/V_{Rossby} (in the absolute values) as a function of λ, where V_x is the westward drift velocity and V_{Rossby} is the Rossby velocity (13). Open symbols correspond to various anticyclones generated in layers of different thickness H_0. Black dots and the solid line fit are the theoretical values derived from the Nycander centre-of-mass velocity formula for the large-scale vortices.

different depths do not match. Indeed, for the same value of $\lambda \approx 1$ we get three values of the ratio V_x/V_{Rossby}: 0.75, 0.95 or 1.3 corresponding, respectively, to depths equal to 12, 6 or 4 mm. This is an indication that the Rossby velocity given by (13) does not provide an accurate scaling for the drift velocity of free isolated vortices in the paraboloidal experiment. A possible reason for that could be related to corrections due to non-trivial topographic effects in paraboloidal geometry which are neglected in (13). Indeed, we found that these effects may slightly change the ratio V_x/V_{Rossby} but, nevertheless, the results for different depths still do not match. A possible explanation of this discrepancy is that finite-size effects and finite horizontal curvature of the vessel become important for vortices which are that large. To take them properly into account a fully curvilinear (cf. Romanova & Zeitlin 1984) analysis of this problem is necessary. This will be done elsewhere.

Let us add that, unfortunately, a systematic quantitative comparison of our results with those obtained for isolated vortex drift velocities by Nezlin & Snezhkin (1993) was not possible because the parameter which is most important for vortex identification, elevation, was not measured by these authors.

4.4. *Cyclone–anticyclone asymmetry*

In order to obtain large-scale cyclones and compare their dynamical properties with large-scale anticyclones, we used the generation technique described in figure 4(*b*). For obvious reasons, we were unable to obtain cyclones with a relative elevation parameter larger than $\lambda = 1$. In fact we could not move beyond $\lambda = 0.75$. Therefore, a direct comparison with anticyclones of strong elevation is impossible. Figure 16(*a*) shows the evolution of a large-scale axisymmetric cyclone. This cyclone stays circular and propagates westwards with a small northward drift. According to the data plotted in figure 14, the absolute values of the northward drift of cyclones are equal to the

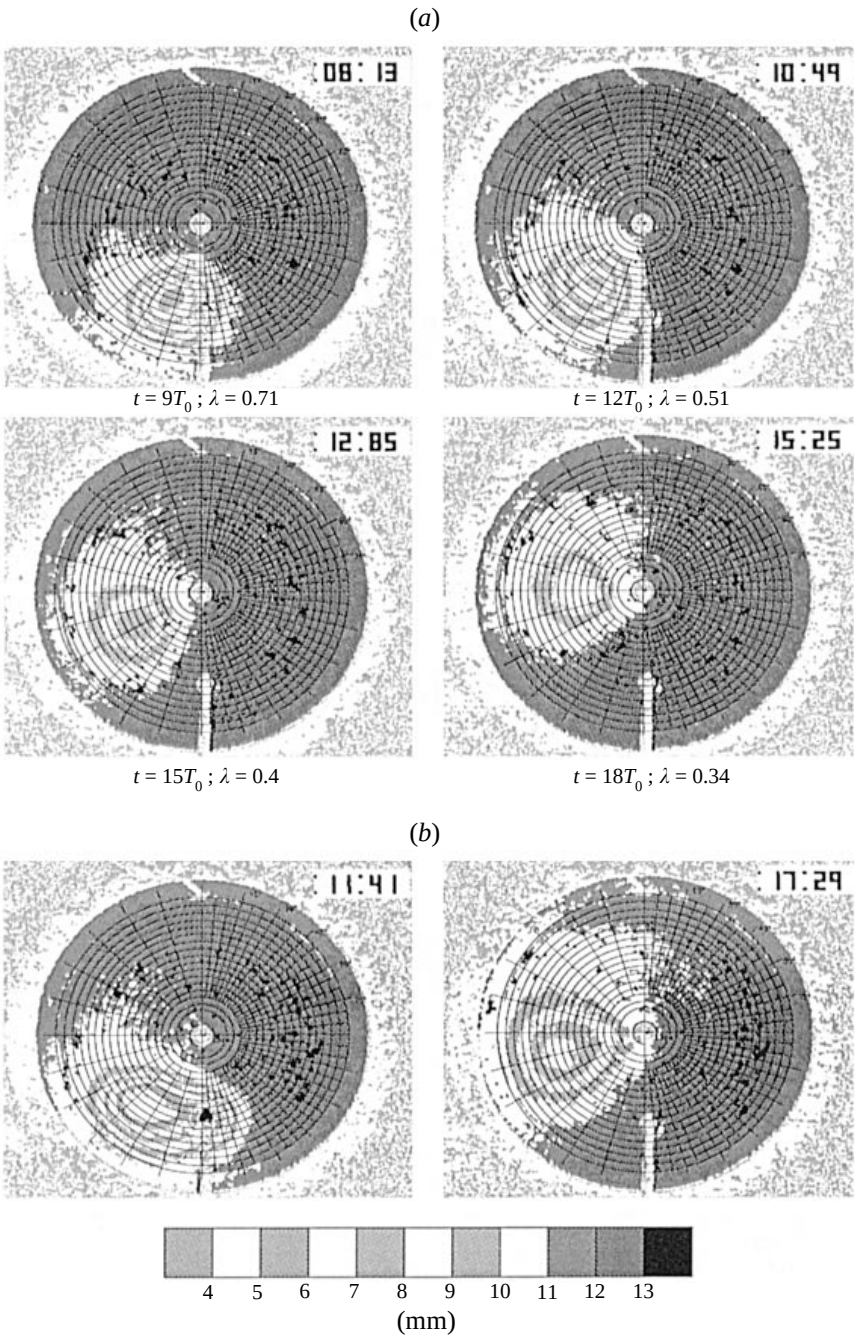

FIGURE 16. Topographic maps of the free surface for (*a*) initially axisymmetric and (*b*) initially elliptic cyclones. The unperturbed layer thickness is $H_0 = 12.5$ mm, the period of rotation of the vessel is $T_0 = 0.842$ s. The characteristic horizontal scale $L_0 = 4.5$ cm is slightly larger than the Rossby radius $R_{Rossby} = 2.8$ cm, but not as large as for the large-scale anticyclone in figure 9.

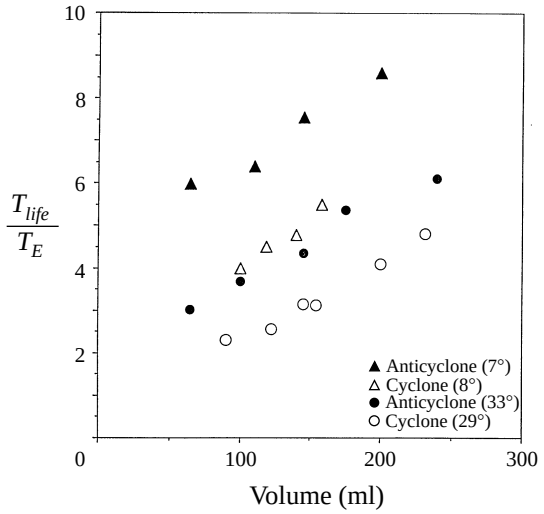

FIGURE 17. Lifetimes of cyclones and anticyclones as a function of sucked (cyclones) or injected (anticyclones) volume in the unperturbed layer $H_0 \approx 2$ mm. The two largest cyclones (200 ml and 230 ml) generated at $\theta \approx 29°$ were initially elliptic (cf. figure 16*b*). The other cyclones are axisymmetric. Lifetimes are rescaled by the standard Ekman spin-down time (15). Filled symbols represent anticyclones and open symbols cyclones. Circles correspond to the vortices generated at $\theta \approx 29°$, while vortices generated close to the centre are denoted by triangles.

southward drift of anticyclones having the same relative elevation parameter. Hence, the large-scale cyclones obtained in our experiment manifest the quasi-geostrophic behaviour as well as the anticyclones of the same relative amplitude.

When we tried to get a larger cyclone by increasing the amount of sucked liquid, we obtained, in the initial stage, an elliptic vortex, as shown in figure 16(*b*). Indeed, owing to the beta-effect, a part of the vortex began to drift westwards while the fluid was still being sucked at the location of the pipe. This process naturally creates a cyclone elongated in the westward direction. However, this structure tends to become symmetric after a few revolutions.

In parallel with the above-described study of anticyclones, we investigated the lifetimes of cyclones drifting at $\theta \approx 30°$ colatitude where the beta-effect is maximal and compared them with the lifetimes of cyclones generated at the centre of the vessel where there is no beta-effect. The results of this analysis are shown in figure 17. In addition, we plot in this figure data obtained for the anticyclones generated in the same unperturbed layer. For intermediate relative elevations ($0.4 < \lambda < 0.75$) the lifetimes of cyclones decrease when the beta-parameter increases $T_{life(30°)} \approx 0.4 T_{life(centre)}$. Here, again, these cyclones, like anticyclones of the same relative amplitude, manifest a quasi-geostrophic behaviour, the lifetimes of vortices drifting at $\theta \approx 30°$ being reduced by the Rossby wave emission/dispersion.

Like in the previous experiments with a paraboloidal vessel with a thin layer (Antipov *et al.* 1981; Nezlin & Snezhkin 1993) we observed that for a given size the lifetime of a cyclone is less than the lifetime of an anticyclone. However, unlike the preceding authors, we investigate this cyclone–anticyclone asymmetry close to the centre of the vessel, as well. We observed, see figure 17, that this asymmetry still exists near the centre, where the beta-effect vanishes. Indeed, by going from $\theta \approx 30°$ to $\theta \approx 7°$ we reduce the beta-parameter by a factor three while differences in lifetimes between cyclones (open circles) and anticyclones (filled circles) are always about 30 %–

40%. Hence, the asymmetry in lifetimes between cyclones and anticyclones is not related to the beta-effect.

The question of the cyclone–anticyclone asymmetry thus requires further investigation. Three possible mechanisms may be responsible for this phenomenon, in our view. First, as far as dissipation is concerned, the nonlinear effects may accelerate the Ekman spin-down of cyclones, although this was shown for small-scale ($L \ll R_{Rossby}$) vortices only (Kloosterziel & van Hejst 1992). Second, in spite of the fact that we see no clear instability manifestations in our experiments, we cannot completely exclude this possibility. Indeed, it was shown numerically by Cushman-Roisin & Tang (1990) that large-scale cyclones in the frontal dynamics regime are unstable on the *f*-plane. Third, numerical simulations of Polvani *et al.* (1994) show that the cyclone–anticyclone asymmetry is present in freely decaying inviscid shallow-water turbulence on the *f*-plane and becomes more pronounced when the Froude number grows. This means that geostrophically unbalanced motions could play a role in establishing the asymmetry in question. A detailed analytical and experimental investigation of this problem for large-scale ($L \gg R_{Rossby}$) vortices is in progress now (Poux 1997).

5. Conclusions

Thus, by performing experiments with isolated large-scale vortices we have demonstrated that two different dynamical regimes exist in the rotating paraboloidal shallow-water layer. They are governed by the characteristic nonlinearity of the vortex and are consistent with the standard quasi-geostrophic and strongly nonlinear (frontal dynamics) regimes predicted by the intermediate balanced models. When the relative elevation parameter changes we observe a continuous transition from one regime to another, concerning the pattern of the vortex behaviour. Quantitatively, at relative elevations less than 0.4 we clearly observe the standard quasi-geostrophic evolution, at relative elevations greater than 1 we clearly see the strongly nonlinear evolution, and in between the intermediate behaviour is observed. In the range of parameters where both cyclones and anticyclones may exist we observe asymmetry in their lifetimes consistent with the previous studies (Nezlin & Snezhkin 1993). However, we prove experimentally that this asymmetry persists in the absence of the beta-effect and, thus, is not related to the Rossby wave radiation. We also show that vortex lifetimes in the strongly nonlinear regime are not sensitive to changes of β while this is the case for the quasi-geostrophic regime. The measurements of the drift velocities of the vortices exhibit deviations from the infinite beta-plane predictions and, for the moment, we are not able to give a satisfactory explanation of this discrepancy. One possible reason is the finite size and finite horizontal curvature effects both necessitating inclusion of curvature effects and resulting in changes in boundary conditions with respect to the infinite beta-plane analysis.

The two basic regimes observed in experiments differ substantially concerning vortex longevity, its coherence and transport properties and its drift direction. However, the characteristic scales of vortices in both regimes are not very different. For example, we see a typical nonlinear behaviour starting from $L_0 \geqslant 3R_{Rossby}$. Hence, to understand the dynamics of a structure which is just two or three times larger than the characteristic Rossby scale it may be necessary to use a non-standard intermediate model.

We should emphasize, however, that in the framework of asymptotic intermediate models when $\beta \approx \epsilon \ll 1$, $\lambda \approx 1$ a strongly nonlinear regime (Stegner & Zeitlin 1995, 1996) in a paraboloidal geometry allows long-lived monopolar vortices while this is not

the case in the frontal dynamics regime (Williams & Yamagata 1984; Cushman-Roisin (1986) in the planetary geometry. Therefore, comparisons of the large-scale strongly nonlinear vortices obtained in the laboratory with atmospheric or oceanic ones should be done with care. In any case, the present experimental device allowing simultaneous study of the beta-plane and the *f*-plane phenomena may be used to model a number of geophysical hydrodynamic situations and, in particular, to provide further tests of the predictions of the balanced models.

The participation of Y. Couder at all stages of this work is gratefully acknowledged. We benefited much from his vast experience as well as from the logistic support at his laboratory at LPS. We thank H. Thome and J. Olejnick for their contribution in the design of the experimental apparatus and to M. Manghi for his valuable collaboration in the experiment. We are grateful to M. V. Nezlin for stimulating discussions and comparisons of the experimental results during his visit to LPS and to X. Carton, B. Legras and P. Tabeling for useful discussions. A.S. thanks J. J. Rasmussen and B. Stenum for fruitful interactions during his visit to Risø (Roskilde). We are grateful to anonymous referees for their helpful remarks. This research was supported in part by the GdR CNRS-IFREMER-SHOM 'Mécanque des Fluides Géophysiques et Astrophysiques'.

REFERENCES

Antipov, S. V., Nezlin, M. V., Snezhkin, E. N. & Trubnikov, A. S. 1981 Rossby solitons. *JETP Lett*. **33**, 351–355.

Brundage, W. L. & Dugan, J. P. 1986 Observations of an anticyclonic eddy of 18° water in the Sargasso Sea. *J. Phys,. Oceanogr*. **16**, 717–727.

Busse, F. H. 1994 Convection driven zonal flows and vortices in the major planets. *Chaos* **4**, 123–134.

Carnevale, G. F., Kloosterziel, R. C. & Heijst, G. J. F. van 1991 Propagation of barotropic vortices over topography in a rotating tank. *J. Fluid Mech*. **233**, 119–139.

Cushman-Roisin, B. 1986 Frontal geostrophic dynamics. *J. Phys. Oceanogr*. **16**, 132–143.

Cushman-Roisin, B. & Tang, B. 1990 Geostrophic turbulence and emergence of eddies beyond the radius of deformation. *J. Phys. Oceanogr*. **20**, 97–102.

Ebbesmeyer, C. C., Taft, B. A., McWilliams, J. C. *et al*. 1986 Detection, structure, and origin of extreme anomalies in a western Atlantic oceanographic section. *J. Phys. Oceanogr*. **16**, 591–612.

Firing, E. & Beardsley, R. C. 1976 The behavior of a barotropic eddy on a beta-plane. *J. Phys. Oceanogr*. **6**, 57–65.

Kloosterziel, R. C. & Hejst, G. J. F. van 1992 The evolution of stable barotropic vortices in a rotating free-surface fluid. *J. Fluid Mech*. **239**, 607–629.

Kukharkin, N. & Orszag, S. A. 1996 Generation and structure of Rossby vortices in rotating fluids. *Phys. Rev*. E **54**, 4524–4527.

Lai, D. Y. & Richardson, P. L. 1977 Distribution and movement of Gulf-Stream rings. *J. Phys. Oceanogr*. **7**, 670–683.

Mac Low, M. M. & Ingersoll, A. P. 1986 Merging of vortices in the atmosphere of Jupiter: An analysis of voyager images. *Icarus* **65**, 353–369.

McWilliams, J. C. & Flierl, G. R. 1979 On the evolution of isolated, nonlinear vortices. *J. Phys. Oceanogr*. **9**, 1155–1182.

McWilliams, J. C. & Gent, P. R. 1980 Intermediate models of planetary circulations in the atmosphere and ocean. *J. Atmos. Sci*. **37**, 1657–1678.

Marcus, P. S. 1990 Vortex dynamics in a shearing zonal flow. *J. Fluid Mech*. **215**, 393–430.

Masuda, A., Marubayashi, K. & Ishibashi, M. 1990 A laboratory experiment and numerical simulation of an isolated barotropic eddy in a basin with topographic β. *J. Fluid Mech*. **213**, 641–659.

Meyers, S. D., Sommeria, J. & Swinney, H. L. 1989 Laboratory study of the dynamics of jovian-type vortices. *Physica* D **37**, 515–530.

Mied, R. P. & Lindemann, G. R. 1979 The propagation and evolution of cyclonic Gulf Stream rings. *J. Phys. Oceanogr.* **9**, 1183–1206.

Mikhailova, E. N. & Shapiro, N. B. 1980 A two-dimensional model of the evolution of synoptic disturbances in the ocean. *Atmos. Ocean Physics-Izv.* **16**, 823–830.

Nezlin, M. V., Rylov, A. Yu., Titishov, K. B. & Chernikov, G. P. 1996 Inverted cyclonic-anticyclonic asymmetry of the solitary Rossby vortices under the presence of a gradient in the rotating shallow water in the paraboloid. *Atmos. Ocean Phys.-Izv.* (in press).

Nezlin, M. V. & Snezhkin, E. N. 1993 *Rossby Vortices, Spiral Structure, Solitons*. Springer.

Nycander, J. 1993 The difference between monopole vortices in planetary flows and laboratory experiments. *J. Fluid Mech.* **254**, 561–577.

Pedlosky, J. 1987 *Geophysical Fluid Dynamics*. Springer.

Petviashvili, V. I. 1980 Red spot of Jupiter and the drift soliton in a plasma. *JETP Lett.* **32**, 619–622.

Polvani, L. M., McWilliams, J. C., Spall, M. A. & Ford, R. 1994 The coherent structures of shallow-water turbulence: Deformation radius effects, cyclone/anticyclone asymmetry and gravity-wave generation. *Chaos* **4**, 177–186.

Poux, C. 1977 Nonlinear effects in the Ekman spin-down of an isolated vortex. Memoire DEA (master thesis), University Paris 6.

Rasmussen, J. J., Stenum, B. & Snezhkin, E. N. 1996 Drift velocities of forced vortices in rotating shallow water. Talk given at the Vortex Dynamics session of the EGS Congress (Den Haag, Netherlands).

Read, P. L. & Hide, R. 1983 Long-lived eddies in the laboratory and in the atmosphere of Jupiter and Saturn. *Nature* **302** (10), 126–129.

Reznik, G. M. & Dewar, W. K. 1994 An analytic theory of distributed axisymmetric barotropic vortices on the β-plane. *J. Fluid Mech.* **269**, 301–321.

Romanova, N. N. & Zeitlin, V. 1984 On quasigeostrophic motions in barotropic and baroclinic fluids. *Atmos. Ocean Physics-Izv.* **20**, 85–91.

Romanova, N. N. & Zeitlin, V. 1985 Solitary Rossby waves in a weakly stratified medium. *Atmos. Ocean Physics-Izv.* **21**, 627–630.

Smith, B. A., Soderblom, L., Johnson, T. V. *et al.* 1979 The Jupiter system through the eyes of Voyager-1. *Science* **204**, 951–972.

Smith, B. A., Soderblom, L., Batson, R. *et al.* 1982 A new look at the Saturn system: The Voyager-2 images. *Science* **215**, 504–537.

Smith, B. A., Soderblom, L., Banfield, D. *et al.* 1989 Voyager 2 at Neptune: imaging science results. *Science* **246**, 1422–1449.

Sommeria, J. Nore, C., Dumont, T. & Robert, R. 1991 Statistical theory of the Great Red Spot of Jupiter. *C.R. Acad. Sci.* II **312**, 999–1005.

Stegner, A. & Zeitlin, V. 1995 What can asymptotic expansions tell us about large-scale quasi-geostrophic anticyclonic vortices? *Non-linear Processes Geophys.* **2**, 186–193.

Stegner, A. & Zeitlin, V. 1996 Asymptotic expansions and monopolar solitary Rossby vortices in barotropic and two-layer model. *Geophys. Astrophys. Fluid Dyn.* **83**, 159–195.

Sutyrin, G. G. 1985 On the theory of solitary anticyclones in a rotating fluid. *Dokl. Akad. Nauk SSSR*, **280**, 1101–1105 (transl. *Earth Sci.* pp. 38–41).

Sutyrin, G. G. & Flierl, G. R. 1994 Intense vortex motion on the beta-plane; development of the beta-gyres. *J. Atmos. Sci.* **51**, 773–790.

Sutyrin, G. G., Hesthaven, J. S., Lynov, J. P. & Rasmussen, J. J. 1994 Dynamical properties of vortical structures on the beta-plane. *J. Fluid Mech.* **268**, 103–131.

Sutyrin, G. G. & Yushina, I. G. 1988 Formation of vortical soliton. *Dokl. Akad. Nauk SSSR*, **299**, 580–584 (transl. *Sov. Phys. Dokl.* **33** (3), 179–181).

Warn, T., Bokhove, O., Shepherd, T. G. & Vallis, G. K. 1995 Rossby number expansions, slaving principles, and balanced dynamics. *Q.J.R. Met. Soc.* **121**, 723–739.

Williams, G. P. 1985 Geostrophic regimes on a sphere and a better plane. *J. Atmos. Sci.* **42**, 1237–1243.

Williams, G. P. & Yamagata, T. 1984 Geostrophic regimes, intermediate solitary vortices and Jovian eddies. *J. Atmos. Sci.* **41**, 453–478.